MNRAS **000**, 1–8 (2020) Preprint March 10, 2022 Compiled using MNRAS LATEX style file v3.0

On the formation of exotic, massive, stellar-remnant black holes at solar and sub-solar metallicities through evolution of massive binaries

Sambaran Banerjee[1,2]★
[1] *Helmholtz-Instituts für Strahlen- und Kernphysik (HISKP), Nussallee 14-16, D-53115 Bonn, Germany*
[2] *Argelander-Institut für Astronomie (AIfA), Auf dem Hügel 71, D-53121, Bonn, Germany*

arXiv:1912.06022v1 [astro-ph.SR] 12 Dec 2019

March 10, 2022

ABSTRACT
The recent inference of a $70M_\odot$ black hole (BH) in the Galactic, detached binary LB-1 has sparked cross-disciplinary debate since a stellar remnant of such large mass is well above what can be expected from stellar-evolutionary theory, especially in an enriched environment like that of the Milky Way. This study focusses on the possibilities of formation of extraordinarily massive BHs at solar and globular cluster (GC)-like metallicities via evolution of massive stellar binaries. A population-synthesis approach is followed utilizing the recently-updated `BSE` program. BHs in the mass range of $50M_\odot - 80M_\odot$ could be formed at the solar metallicity only if a large fraction, $\gtrsim 70\%$, of matter is allowed to accrete onto a low-mass BH, in a BH-star merger product (a "black hole Thorne-Zytkow object"; BH-TZO). Their counterparts at GC-like metallicities can reach $100M_\odot$. Although post-accretion BHs can, generally, be expected to be of high spin parameter, they can potentially be of low spin in the case of a BH-TZO. This spin aspect remains speculative in this work and deserves detailed hydrodynamic studies.

Key words: stars: black holes — stars: massive — stars: mass-loss — binaries: general — supernovae: general — methods: numerical

1 INTRODUCTION

The recent discovery of a detached binary in our Galaxy's field, comprising of a $68^{+11}_{-13}M_\odot$ black hole (hereafter BH) and a B-type star of $8.2^{+0.9}_{-1.2}M_\odot$ in a 78.9-day, near-circular (eccentricity $e = 0.03 \pm 0.01$) orbit, as inferred by Liu et al. (2019) through radial-velocity measurements, has become a focal topic across disciplines in astronomy. While other detached BH-star binaries have also been discovered over the last couple of years in Galactic globular clusters (hereafter GC) and in the field (Giesers et al. 2018, 2019; Thompson et al. 2019), the above binary, nicknamed LB-1, is much of an exception due to its BH member's $\approx 70M_\odot$ mass. As opposed to this, the BH members of all the other, to-date known Galactic BH-star binaries are estimated to be of $< 10M_\odot$ (the unseen member in the APOGEE binary of Thompson et al. 2019 can, in fact, be an exceptionally-massive neutron star; hereafter NS).

Note that LIGO-Virgo observations of gravitational waves (hereafter GW) from binary black hole (hereafter BBH) mergers have, so far, identified up to $\approx 50M_\odot$ BH (Abbott et al. 2019), which, after taking into account the measurement uncertainties, is consistent with the $\approx 40M_\odot$ upper limit expected for stellar-remnant BHs due to pulsation pair-instability supernova (Langer et al. 2007; Woosley 2017). From that point of view, a $70M_\odot$ BH is indeed intriguing but can potentially be explained as a BBH merger product (*e.g.*, Rodriguez et al. 2016; Banerjee 2017; Di Carlo et al. 2019) or as the remnant of a star-star merger (*e.g.*, Banerjee et al. 2019; Spera et al. 2019). However, such merger-based scenarios would still require sub-solar metallicities, given that at the solar metallicity single-stellar evolution would yield up to $\approx 15M_\odot$ BH even for a very large zero age main sequence (hereafter MS; ZAMS) mass (Hurley et al. 2000; Belczynski et al. 2010; Banerjee et al. 2019), as per the current understanding of stellar wind mass loss. Therefore, the finding of a $70M_\odot$ BH in the Milky Way's field clearly presents challenges to our current understanding of stellar evolution. Note that LB-1's observed spectral variability is, as well, susceptible to alternative interpretations that would point to a much lower mass of its invisible member (El-Badry & Quataert 2019; Abdul-Masih et al. 2019).

In this context, this work follows a population synthesis-based approach to investigate the conditions, however exotic

★ E-mail: sambaran@astro.uni-bonn.de (SB)

© 2020 The Authors

they may be, under which BHs of $50M_\odot - 80M_\odot$ can form in solar-metallicity (or near-solar-metallicity) environments. In particular, observationally-motivated massive binary populations are evolved, using an updated version of the BSE binary-evolution program, to study their remnant outcomes. The possibilities and mechanisms for forming such massive BHs at low metallicities are also explored. This paper is organized as follows: Sec. 2 describes the BSE program, the model massive-binary population, and the adopted physical conditions. Sec. 3 describes the results. Sec. 4 discusses the caveats, outlooks, and future prospects.

2 METHOD: POPULATION SYNTHESIS WITH THE UPDATED BSE

The binary-evolution program BSE (Hurley et al. 2002) and its single-stellar evolutionary counterpart SSE (Hurley et al. 2000) are utilized to evolve the massive binary population and the single massive stars (see below). SSE and BSE are fast, semi-analytical, recipe-based programs that are widely utilized for stellar population synthesis. They also serve as stellar evolution engines in widely used N-body simulation programs such as NBODY6, NBODY7 , NBODY6++, MOCCA, and CMC (Aarseth 2003, 2012; Wang et al. 2015; Hypki & Giersz 2013; Joshi et al. 2000). SSE and BSE share the same single stellar evolution prescriptions but BSE incorporates additional recipes describing the binary-interaction physics (tidal interaction, mass transfer, common-envelope evolution, coalescence, general-relativistic orbit inspiral) and the binary-orbital mechanics; see Hurley et al. (2002) for the details. Here, an amended version of the original BSE, as described in Banerjee et al. (2019), is utilized.

To summarize, the amendments are in the SSE sector with updates of the stellar wind according to the recipes of Belczynski et al. (2010, hereafter B10), of the stellar remnant formation according to the "rapid" and "delayed" prescriptions of Fryer et al. (2012, hereafter F12), and the implementations of pulsation pair-instability supernova (hereafter PPSN) and pair-instability supernova (hereafter PSN) recipes as per Belczynski et al. (2016, hereafter B16). Material fallback and neutrino mass loss (neutrino mass loss according to Lattimer & Yahil 1989 for an NS remnant, assumed 10% here for a BH remnant) are taken into account in implementing the final NS or BH remnant mass. The fallback fraction is also explicitly considered while implementing the natal kick of an NS or a BH based on the "momentum-conserving" principle as in Belczynski et al. (2008, hereafter B08). Alternatives of the momentum-conserving kick, *e.g.*, "collapse-asymmetry-driven" and "neutrino-emission-driven" kicks are also kept as possibilities. The binary-evolution physics remains the same as in Hurley et al. (2002) along with its subsequent amendments that are available in the public versions of BSE. The original SSE recipes of Hurley et al. (2000) and its earlier amendments are also retained and the above, newest recipes can be opted for via appropriate option flags. That way, SSE and BSE now offer a wide range of situations for exploring in stellar-evolutionary population synthesis that are based on current understandings in stellar evolution and remnant formation, being at par and in near-perfect agreement (Banerjee et al. 2019) with contemporary population synthesis programs such as StarTrack (Belczynski et al. 2008). Similar ingredients are available also in the BSE-derivative MOBSE (Giacobbo et al. 2018) and the triple evolution program TrES (Toonen et al. 2016).

Two additional parameters are introduced in the binary population evolution conducted here. First, a constant mass-loss fraction, $f_{\rm mrg}$, with respect to the less massive member (as of just before the merger) during a star-star merger process. Secondly, a constant mass-accretion fraction, $f_{\rm TZ}$, onto a BH when it coalesces with a star, forming a "BH Thorne-Zytkow object" (hereafter BH-TZO). The corresponding accretion fraction on to an NS Thorne-Zytkow object (Thorne & Zytkow 1975, hereafter NS-TZO) is assumed to be always zero, as defaulted in BSE[1]. Of course, the constancy of $f_{\rm mrg}$ and $f_{\rm TZ}$ is an oversimplification which quantities, in reality, would depend on poorly understood or explored details of these processes. Here, they simply serve as convenient parametrizations of star-star merger mass loss and BH-TZO accretion. Unless stated otherwise, the B10 stellar wind, F12-rapid remnant formation plus B16-PPSN/PSN, and momentum-conserving natal kick recipes are applied throughout this work (the one-dimensional natal kick dispersion of a $1.4M_\odot$ NS is taken to be 265 km s^{-1}; Hobbs et al. 2005). Based on hydrodynamic studies of stellar mergers (*e.g.*, Gaburov et al. 2008; de Mink et al. 2013; De Mink et al. 2014), $f_{\rm mrg} = 0.2$ (*i.e.*, $\leq 10\%$ loss from the total mass budget during a star-star merger) is adopted throughout. The cases of $f_{\rm TZ} = 0.0$, 0.5, 0.7, and 0.9 are explored and as well those of the common envelope (CE) efficiency parameter $\alpha = 1.0$, 3.0 and 5.0. The solar metallicity is taken to be $Z = Z_\odot = 0.02$, as defaulted in SSE. Also, as noted in Banerjee et al. (2019), the SSE time step parameters of (pts1,pts2,pts3) = (0.001,0.01,0.02) are applied to achieve stability and convergence.

With the above settings, 10^4 massive, O-type binaries are evolved. The binaries initially follow the orbital-period, eccentricity, and mass-ratio distributions of Sana & Evans (2011) that represent the observed population of O-star binaries in young clusters and the field. The ZAMS masses of the individual binary members are drawn from the Kroupa (2001) initial mass function (IMF) over the mass ranges $20.0M_\odot - 150.0M_\odot$ or $20.0M_\odot - 200.0M_\odot$. Motivated by the $> 150M_\odot$ initial mass inferred for single stars in young massive clusters (*e.g.*, Crowther et al. 2010), the somewhat higher stellar upper mass limit, $m_{\rm max}$, is considered along with its canonical value of $m_{\rm max} \approx 150M_\odot$ (Weidner & Kroupa 2004). The binary populations are generated with the McLuster program (Küpper et al. 2011).

3 RESULTS

Fig. 1 shows the resulting ZAMS mass - remnant mass relations for the different values of $f_{\rm TZ}$ and α as indicated on the panels. On each panel, when a binary yields a single remnant, its primary's (the member with larger ZAMS mass) ZAMS mass, M_1, is plotted along the x-axis. If a binary evolves to yield two remnants then the ZAMS masses of their parent stars are correspondingly plotted along the x-axis. The BH mass and its uncertainty (90%), as inferred in

[1] These parameters are starightforwardly implemented in the subroutine MIX.

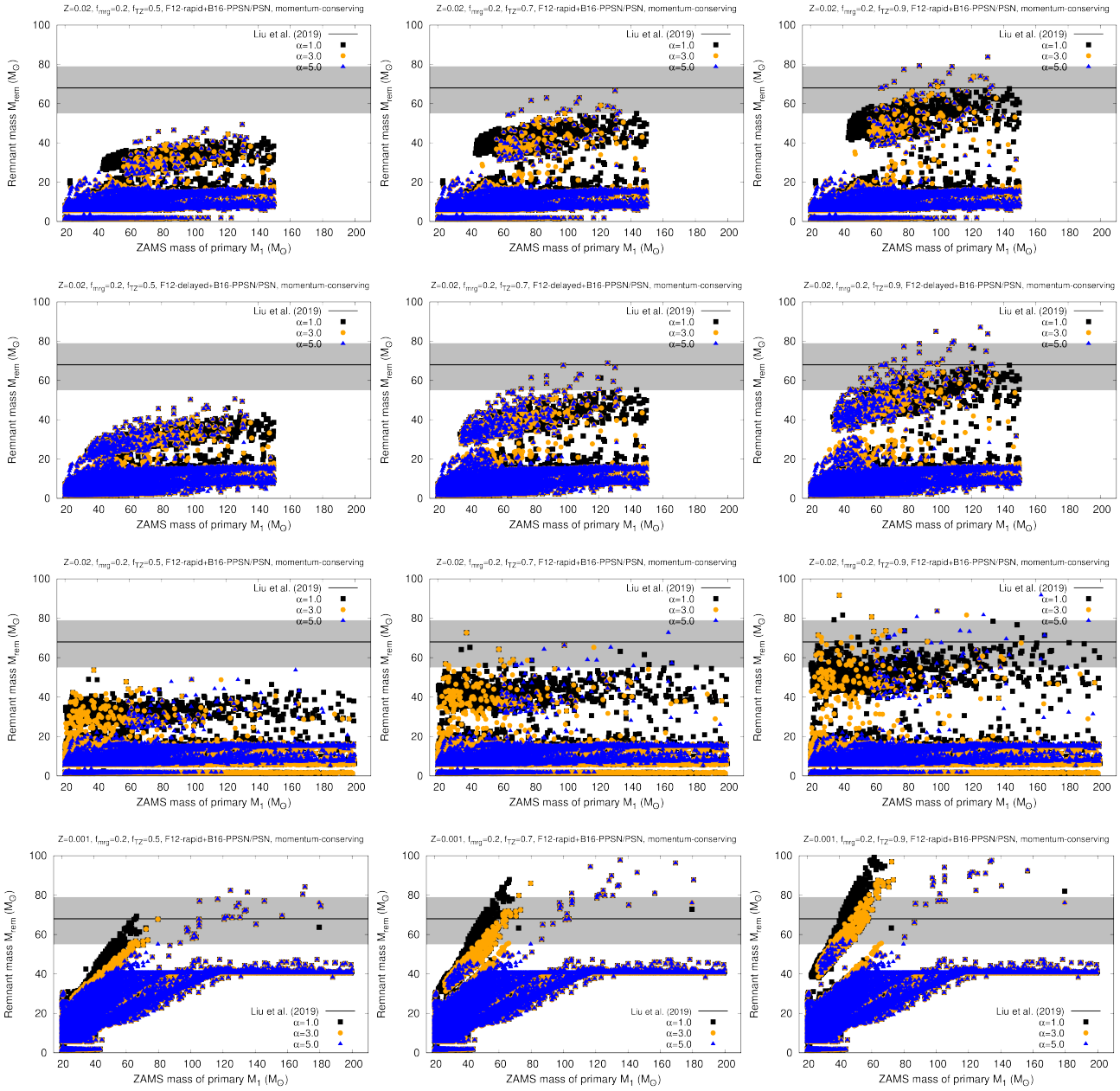

Figure 1. Zero age main sequence (ZAMS) mass-remnant mass relations for the massive-binary population evolution modelled in this work (comprising 10^4 massive binaries; see Sec. 2), for the different "black hole Thorne-Zytkow object accretion fraction", $f_{\rm TZ}$, star-star merger mass loss fraction, $f_{\rm mrg}$, and common envelope (CE) efficiency parameter α as indicated in the panels' legends. For each panel, when a binary yields a single remnant, its primary's (the member with larger ZAMS mass) ZAMS mass is plotted along the x-axis. If a binary evolves to yield two remnants then the ZAMS masses of their parent stars are correspondingly plotted along the x-axis. The evolutions shown here assume the F12-rapid remnant formation model along with the PPSN/PSN model of B16 (Sec. 2) except for those on the second row which correspond to the F12-delayed remnant model (Sec. 2). All panels correspond to the metallicity $Z = Z_\odot = 0.02$ except for those on the fourth row for which $Z = 0.05 Z_\odot$. The inferred black hole mass of LB-1 binary (black, solid line) and its uncertainty (90%; grey, shaded region) by Liu et al. (2019) are indicated on each panel. See Fig. 2 for the ZAMS mass-remnant mass relation for the corresponding single stellar evolution.

the observations of LB-1 by Liu et al. (2019), are also shown on each panel. It can be seen that for $f_{\rm TZ} = 0.7$, BHs up to $\approx 70 M_\odot$ are formed at $Z = 0.02$ for both the $m_{\rm max} = 150 M_\odot$ and $200 M_\odot$ binary populations, for both F12-rapid and F12-delayed remnant-formation models, and for $\alpha = 1.0$, 3.0, and 5.0. For $f_{\rm TZ} = 0.9$ and $Z = 0.02$, the maximum BH mass exceeds $80 M_\odot$ ($90 M_\odot$) for $m_{\rm max} = 150 M_\odot$ ($m_{\rm max} = 200 M_\odot$). On the other hand, when $f_{\rm TZ} = 0.5$ and $Z = 0.02$ the BH masses do not reach even the lower bound of the LB-1 value ($55 M_\odot$) for $m_{\rm max} = 150 M_\odot$ and marginally reaches the value for $m_{\rm max} = 200 M_\odot$. Overall, with a sufficiently large BH-TZO accretion ($\gtrsim 70\%$) the formation of LB-1-like BHs can hap-

pen even at solar-like metallicities and with $\gtrsim 90\%$ accretion both the lower and upper mass bounds of LB-1's BH can be easily accommodated.

At low metallicities, BH masses can grow even larger. For example, at $Z = 0.001$ (typical metallicity of Milky Way GCs), the LB-1 BH mass can be covered even at $f_{\rm TZ} = 0.5$ and for $f_{\rm TZ} = 0.7$ and 0.9, BH masses exceed $100 M_\odot$ (see Fig. 1, fourth row). Note that in all these evolutionary calculations, the B10 wind is applied at its full unlike in recent works such as that of Belczynski et al. (2019) where a reduced wind is applied (but see below). These exotic, high BH masses at solar and lower metallicities occur due to the assumed significant BH-TZO accretion. This is clear from Fig. 1 as one scans the panels from left to right (increasing $f_{\rm TZ}$) along a particular row. With such $f_{\rm TZ}$, although the most massive BHs form via BH-TZO accretion, BBH and NS-BH mergers also contribute to the overall, broad mass spectrum of the BHs that is derived from the binary-population evolution (see below).

It would be worthwhile to investigate what sort of binary interaction(s) lead to such exotic BH masses, especially at the solar metallicity. Examples 1a and 1b of Appendix A demonstrate (via standard `BSE` summary output) such evolutionary channels whose final outcomes are a single BH of $68.8 M_\odot$ and $91.7 M_\odot$ respectively. Here, the more ZAMS-massive member (the primary) starts a Case-A mass transfer as it expands near the end of its MS lifetime, it being inside a close binary. The mass transfer causes the secondary to gain mass significantly, thereby rejuvenating its hydrogen fuel (complete mixing is assumed in `BSE`; see Hurley et al. 2002) and prolonging its MS life (the secondary essentially becomes a blue straggler). This continues until the mass donor has lost all of its hydrogen envelope (due to wind loss plus the mass transfer) to become a helium main sequence star (`K2`$= 7$; a Wolf-Rayet star) and, therefore, shrinks to a large extent, detaching the binary. Note that although the mass ratio has reversed by now, we will continue to refer to the more ZAMS-massive member as the primary. Finally, when the primary's He-core becomes a low-mass BH, it receives a moderate natal kick whose value (as well as the BH's mass at birth of $5.7 M_\odot$) is determined by the (partial; $\approx 60\%$ by mass) fallback (see the kick information at the beginning of Examples 1a & 1b; F12-rapid remnant model and momentum-conserving kick are assumed here). This, in turn, causes the binary to become highly eccentric (but still remain bound), leading to an in-orbit coalescence of the BH with its mass-gainer companion, the formation of a BH-TZO, and, finally, the mass gain of the BH depending on $f_{\rm TZ}$. In other words, the primary "secures" some of its mass with its secondary by transferring material on to and rejuvenating the latter and then gains it back, after becoming a low-mass BH, by merging with it. In these examples, the large mass gain of the BH is due to the adopted $f_{\rm TZ} = 0.9$, as clarified at the end of the corresponding `BSE` outputs. Note that the moderate natal kick of the BH, due to the partial fallback, plays an important role in this scenario by inducing a prompt merger; a full NS-like kick would have likely disrupted such a binary while with too small a kick (*e.g.*, in a collapse-asymmetry-driven kick scenario; Banerjee et al. 2019), one would need to wait for the secondary to become a giant until it fills its Roche lobe and the outcome would become α-dependent ($\alpha = 3.0$ is mentioned for completeness but it has no real role in this evolutionary channel) and, also, the stellar companion may lose a good part of its mass in the mean time to its strong winds at the solar metallicity.

Fig. 2 shows the remnant masses without any BH-TZO accretion ($f_{\rm TZ} = 0$) at $Z = 0.02$, 0.001, and 0.0001, for the $m_{\rm max} = 200 M_\odot$ binary population. Here, LB-1-like and more massive (up to $\approx 80 M_\odot$) BHs appear only at the lower metallicities and in much fewer numbers. In the absence of any BH-TZO accretion, these are the few, most massive BBH merger events. For $Z = 0.02$, the BHs still reach up to $\approx 40 M_\odot$, these being derived, typically, from late-time merger products due to Case-B mass transfer resulting in direct collapse or PPSN. With $f_{\rm TZ} = 0$, star-star mergers or mass accretion episodes from stellar companion produce the majority of the over-massive BHs (with respect to the corresponding single-star ZAMS mass-remnant mass relations as given by the red, solid line in the panels of Fig. 2). The formation of such over-massive BHs via stellar mergers at solar and lower metallicities have also been inferred in other, recent studies, *e.g.*, De Donder & Vanbeveren (2004); Banerjee et al. (2019); Spera et al. (2019). The under-massive BHs, are, on the other hand, the end products of the net mass givers in a binary evolution which are often the primaries.

A striking feature in the $f_{\rm TZ} = 0$, $Z = 0.0001$ case (Fig.2, right panel) is the relatively low-mass ($5.0 \lesssim M_{\rm rem} \lesssim 30.0$) BHs for $M_1 \gtrsim 150 M_\odot$, mostly when $\alpha = 3.0$ and 5.0, and as well the very high mass ($\gtrsim 200 M_\odot$) BHs over the same M_1 range when $\alpha = 1.0$, 3.0, and 5.0. The lower-mass BHs occur in wide, low-mass-ratio systems as in Example 2a of Appendix A. Here, the onset of mass transfer across the components of widely different masses leads to a CE phase and, subsequently, the ejection of the H-envelope of the donor primary, owing to the efficient energy deposition on to the envelope with $\alpha = 3.0$. This results in a tight, detached, symbiotic binary between a helium main sequence (or a naked-helium) primary and the main-sequence secondary. The He-star member, being in between the He-core mass range for PSN ($65.0 M_\odot - 135.0 M_\odot$; see Belczynski et al. 2016; Woosley 2017), leaves no remnant (its wind mass loss is small due to the low Z) while the secondary evolves into a $19 M_\odot$ BH. When $\alpha = 1.0$ (Example 2b of Appendix A), the CE ejection fails (less energy deposition on to the envelope), leading to a merger and the merged star undergoes PSN so that no remnant is left at all. With $\alpha = 3.0$ and the higher $Z = 0.001$ (Example 2c), the evolutionary path is similar to that of Example 2a but, owing to higher wind mass loss, the primary undergoes a PPSN and the secondary becomes an NS instead. Before the NS formation, a stable mass-transfer phase occurs from the secondary to the BH primary, increasing the latter's mass slightly. The binary finally disrupts due to the high natal kick of the NS. It is this type of mass gain via Roche lobe overflow (as opposed to BH-TZO accretion) that leads to the small, preferentially upward spread around the PPSN plateau in the initial-final plots for the low metallicities (Fig. 1, fourth row; Fig. 2, middle and right panels).

On the other hand, the very massive, $\gtrsim 200 M_\odot$ BHs are the outcomes of tight, very massive binaries leading to direct collapse above the PSN mass gap (Spera et al. 2015; Belczynski et al. 2016; Woosley 2017; Giacobbo et al. 2018) as in Example 3a of Appendix A. The star-star merger product, in this case, is sufficiently massive and its wind mass loss is low enough (due to low Z) to yield a BH above the PSN

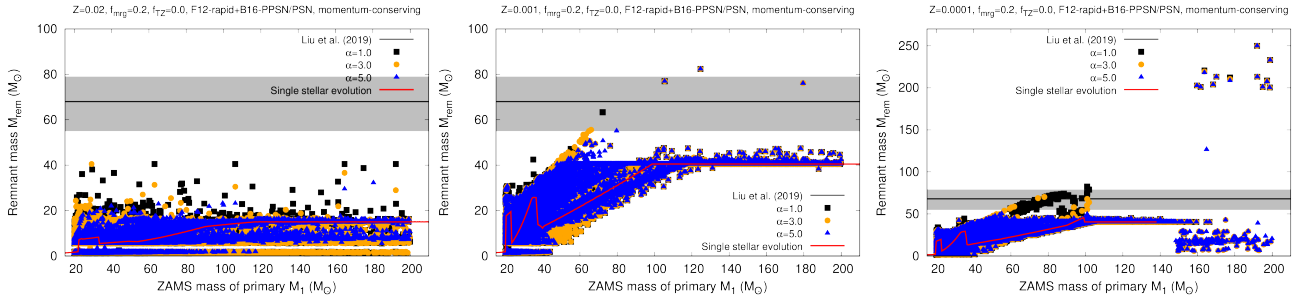

Figure 2. The same as in Fig. 1 but with $f_{\rm TZ} = 0.0$ and for $Z = Z_\odot = 0.02$ (left panel), $Z = 0.05Z_\odot$ (middle), and $Z = 0.005Z_\odot$ (right). The red, solid line on each panel gives the ZAMS mass-remnant mass relation for the corresponding single stellar evolution.

gap (or the "upper" mass gap; *c.f.* Fig. 2, bottom panel of Banerjee et al. 2019).

Fig. 3 shows the number of BHs, at $Z = 0.02$, with $M_{\rm rem} > 40.0M_\odot$, the generally-accepted lower mass limit of a PPSN remnant BH (Belczynski et al. 2016; Woosley 2017), and with $55.0 < M_{\rm rem} < 79.0$, the mass range of the BH in LB-1 as inferred by Liu et al. (2019), as functions of $f_{\rm TZ}$ (the different panels) and α (the x-axes). As expected from Figs. 1 & 2 and the discussions above, $f_{\rm TZ} \gtrsim 0.7$ is necessary to produce such massive BHs. The moderately negative α-dependence is due to the fact that a lower α generally aids in star-star and star-remnant mergers due to the correspondingly longer H-envelope lifetime during a CE phase. Out of the 2×10^4 stellar members (10^4 binaries), the fractional relation with the number of $55.0 < M_{\rm rem} < 79.0$ ($M_{\rm rem} > 40.0M_\odot$) BHs formed is $\approx 1.5\times10^{-2}$ (5.0×10^{-2}), for $f_{\rm TZ} = 0.9$ and $\alpha = 1.0$. For $f_{\rm TZ} = 0.7$, $\alpha = 1.0$ it is $\approx 1.0\times10^{-3}$ (2.5×10^{-2}). These fractions represent lower limits since only 10^4 binaries are evolved in this work; a more robust estimate, which is reserved for a future study, would require $\sim 10^7$ binaries. Note that these numbers correspond to the stellar mass range of $20M_\odot - 200M_\odot$ (for the $m_{\rm max} = 150M_\odot$ binary population, the numbers are marginally lower) and assuming 100% binary fraction over this mass range. With respect to the full, standard IMF, these fractions would easily be $\sim 10^{-2}$ factors lower and even lower for $< 100\%$ binary fractions among O-type stars (the present-day, observed O-star binary fraction is $\approx 50-70\%$; Sana & Evans 2011; Sana et al. 2013).

Finally, Fig. 4 shows the remnant outcomes, for $Z = 0.02$ and $\alpha = 3.0$, when the B10 wind in the evolutionary models is reduced by an arbitrary factor of 0.2. This corresponds to the situation explored recently by Belczynski et al. (2019) with single stellar evolution using `StarTrack` (Belczynski et al. 2008; Belczynski et al. 2016) and `MESA` (Paxton et al. 2011, 2015) programs. The corresponding single-star initial-final relation is shown on the left panel of Fig. 4 (the red, solid line) which resembles that from Belczynski et al. (2019) (their Fig. 2; the maximum BH mass is slightly higher in their case since they assume 1% neutrino mass loss during BH formation as opposed to that of 10% here). As can then be expected, the LB-1 BH mass can be reached even with $f_{\rm TZ} = 0.0$. The very massive, $> 150M_\odot$ BHs in the panels of Fig. 4 are above-PSN-gap BHs as in Fig. 2 (right panel) that is discussed above. They are produced through early mergers of tight, massive binaries where the poor mass loss of the merger product results in a BH above the PSN gap, as demonstrated in Example 3b of Appendix A. If one resets to the full B10 wind, then the same merger product leads to just a $\approx 15M_\odot$ BH (Example 3c of Appendix A) as one expects from such massive ZAMS stars at the solar metallicity (see, *e.g.*, Fig. 1, bottom panels of Banerjee et al. 2019). Note that since the merger happened right at the beginning due to the overlapping initial separation, the $\approx 296M_\odot$ merger product, in this example, is essentially a ZAMS star.

4 DISCUSSIONS AND OUTLOOK

The formation of a merger product (a BH-TZO) between a few-$M_\odot$ BH and a 10s-of-$M_\odot$ stellar object at solar metallicity as in Examples 1a and 1b (Appendix A), staring from a close, massive binary, is, by itself, not exotic and depends mainly on the essentials of binary evolution and orbital mechanics. The details of the `BSE`'s underlying stellar structure do not play a key role up to the BH-TZO formation point. Also, such an outcome happens with the full B10 wind. The exotic aspect is the large amount of mass accretion fraction, $f_{\rm TZ}$, that had to be imposed to grow the BH up to $50M_\odot - 80M_\odot$, the mass limits of the LB-1 BH by Liu et al. (2019). It is unclear if $\gtrsim 70\%$ of mass can be accreted onto the BH from its gaseous cocoon and, even if so, how much time the accretion would take. With $\lesssim 50\%$ BH-TZO accretion, $40M_\odot - 50M_\odot$ BH would still form, but with a very low probability (Fig. 3, Sec. 3).

However, looking from another angle, a large BH-TZO accretion fraction is analogous to the model of BH formation with a large fallback fraction on to a $\sim M_\odot$ proto-remnant (Fryer et al. 2012, and references therein), as adopted in essentially all contemporary population-synthesis and hydrodynamic approaches (*e.g.*, in `BSE`, `MOBSE`, `StarTrack`, and `MESA` programs) for the final remnant formation from an evolved stellar entity. In that respect, the adoption of a large $f_{\rm TZ}$ is as reasonable as BH formation with near-complete fallback of matter onto a several times less massive proto-remnant. The fact that LIGO-Virgo has observed BHs up to $\approx 50M_\odot$ (Abbott et al. 2019) indicates that such fallback-dominated BH formation somehow works out and hence a large $f_{\rm TZ}$ may as well.

Along the same line of argument, the final BH out of a BH-star merger product (which one would normally expect to be of high spin parameter) can, in fact, be of low or practically zero spin parameter, as recently inferred for BH formation from stellar collapse using `MESA` (Belczynski

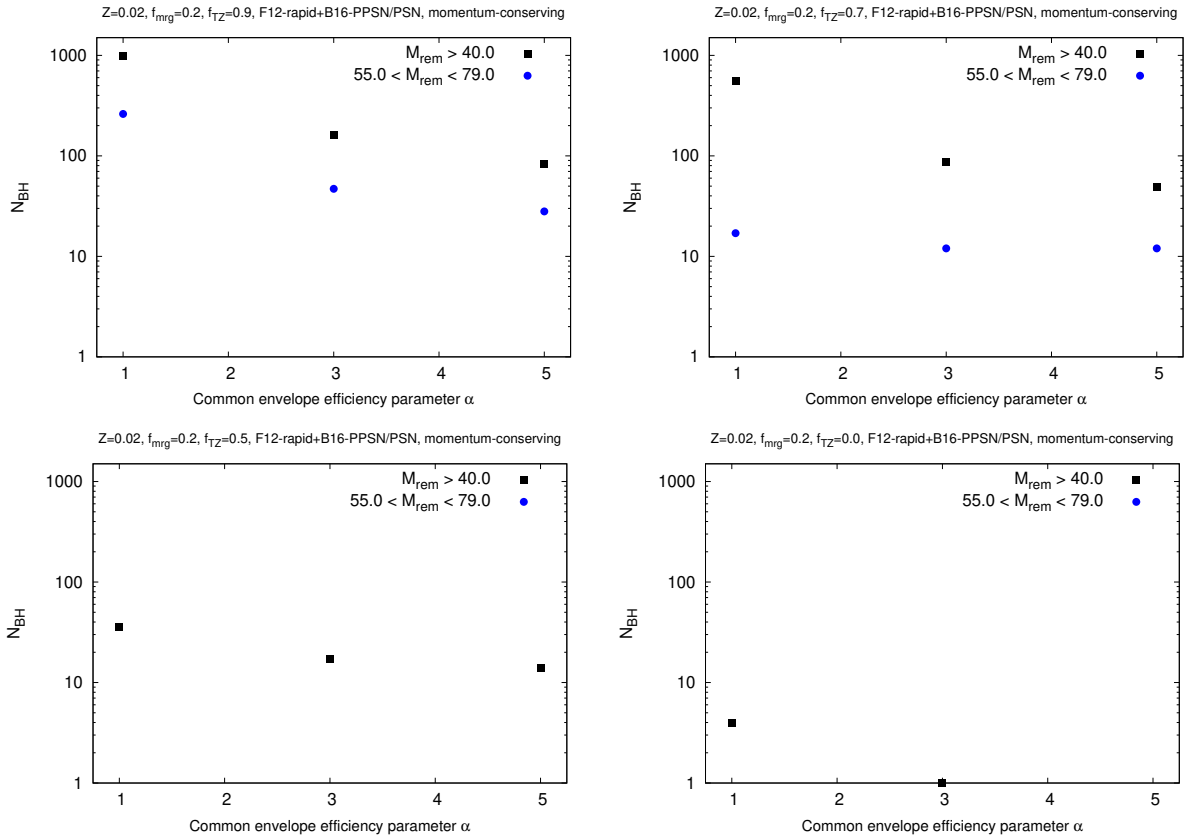

Figure 3. The total numbers of BHs, $N_{\rm BH}$, formed, with $M_{\rm rem} > 40.0 M_\odot$ (the generally-accepted mass of a PPSN remnant BH; black, filled squares) and with $55.0 < M_{\rm rem} < 79.0$ (the mass range of the BH inferred in LB-1; blue, filled circles), out of the 10^4 massive binaries (Sec. 2) as a function of the CE efficiency parameter α. Here, the cases with $f_{\rm TZ} = 0.9$ (top-left panel), 0.7 (top-right), 0.5 (bottom-left), and 0.0 (bottom-right), for $Z = Z_\odot = 0.02$ and $f_{\rm mrg} = 0.2$, are shown. These panels correspond to the outcomes from the population of binaries with components having ZAMS mass up to $200 M_\odot$ (Sec. 2).

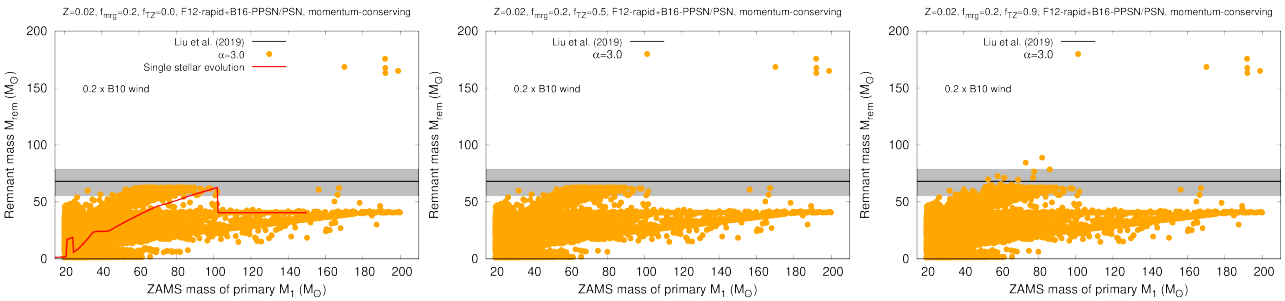

Figure 4. The same as in Fig. 1 but with the stellar wind reduced to 20% of the standard B10 value (Sec. 2) as in Belczynski et al. (2019). Here, the cases with $f_{\rm TZ} = 0.0$ (left panel), 0.5 (middle), 0.9 (right), for $\alpha = 3.0$, $Z = Z_\odot = 0.02$, and $f_{\rm mrg} = 0.2$, are shown. The left panel includes the ZAMS mass-remnant mass relation for the corresponding single stellar evolution (the red, solid line).

et al. 2017). In an evolved star, the angular momentum of the innermost radiative core is carried away outwards (and expelled from the system via the wind) almost entirely, due to the core's strong magnetic coupling with the outer regions caused by the twisting of magnetic field lines threaded into it (Fuller et al. 2019). Given that the BH inside a TZO is also surrounded by a massive cocoon (as opposed to a BH gaining mass from a stellar companion through an accretion disk in which case its spin-up is almost guaranteed), its spin fate may be similar to that of a stellar core. In the case of a BH core, the magnetic field threading and the resulting angular momentum extraction from it would happen relativistically (Blandford & Znajek 1977; Thorne et al. 1986). General relativistic (GR) magnetohydrodynamic (GRMHD) studies are necessary to better understand the fate of such a BH-TZO.

With such BH-TZO accretion, BH mass can reach $\approx 100 M_\odot$ at GC-like metallicities (Fig. 1, fourth row; Sec. 3).

Without any BH-TZO accretion (Fig. 2), BHs barely reach $\approx 40M_\odot$ at $Z = 0.02$ and $\approx 80M_\odot$ for GC-like and lower Z, these being outcomes of late-time star-star mergers or BBH mergers (Sec. 3). These channels operate as well with finite $f_{\rm TZ}$, for all Z. The same applies for mass growth of BHs via accretion from stellar companion.

This work does not address the question how a $\approx 70M_\odot$ BH would acquire a B-type companion. Although the near circular orbit points to an origin from field binary evolution, the key challenge in such a scenario is to avoid merger due to the evolutionary expansion of the BH progenitor. Any evolved BH-progenitor star with H-rich envelope would be much bigger in size than the $\approx 300R_\odot$ ($\approx$ 80-day) orbit of LB-1 (if the LB-1's BH turns out to be of much lower mass, then the orbit would have to be tighter but, depending on the inferred BH mass, one may be able to resort to CE and envelope ejection). It is possible that the BH progenitor evolves chemically homogeneously (De Mink & Mandel 2016; Marchant et al. 2016), maintaining a compact size throughout its lifetime, but then the companion is too far away to circularize any primordial eccentricity through tidal interaction. Although there is evidence of chemical homogeneity in massive BH progenitors in the metal-poor SMC (Ramachandran et al. 2019), it is unclear whether the same would happen for a Milky Way-like enrichment. The binary is also too wide to induce chemical homogeneity in the BH progenitor rotationally (De Mink et al. 2009; Marchant et al. 2016).

Alternatively, the BH can easily be exchanged into a star-star binary in a close encounter inside a low-mass (massive) open cluster (Banerjee 2018), which system can then become a member of the field after the cluster has dissolved (it is ejected from the cluster due to this or subsequent dynamical interaction). This scenario faces difficulty in addressing the near-circular orbit of LB-1, since a dynamically formed and/or ejected binary would have an eccentricity drawn from the thermal distribution (Spitzer 1987). However, with an appropriately-high eccentricity, the orphaned BH-star binary can become symbiotic, circularizing and tightening itself. These possibilities will be investigated in a forthcoming work. See Belczynski et al. (2019) for further possibilities.

This preliminary work has focussed on the most massive BHs formed out of a population of massive binaries. Irrespective of whether LB-1's BH mass would require a revision after follow-up observations or not, such a study is interesting and contextual by its own right. The high (50%-70%) binary fraction among the O-stars in present-day young massive and open clusters suggests similar stellar population in GCs' progenitor clusters. Hence, the properties (BH masses, spins) of dynamically-assembled BBHs and their GR mergers in open and globular clusters would be influenced by the pairing properties of the BHs' progenitor stars. In the near future, larger sets of binary population will be evolved and a detailed study of the resulting remnants' properties (masses and spins) will be made.

ACKNOWLEDGEMENTS

SB acknowledges the support from the Deutsche Forschungsgemeinschaft (DFG; German Research Foundation) through the individual research grant "The dynamics of stellar-mass black holes in dense stellar systems and their role in gravitational-wave generation" (BA 4281/6-1; PI: S. Banerjee). The author acknowledges the discussions with Chris Belczynski, Mirek Giersz (CAMK, Warsaw), Rainer Spurzem, and Peter Berczik (NAOC, Beijing). The motivation for implementing a BH accretion in a BH-star merger product came from an unrelated discussion with Mirek Giersz. SB acknowledges the generous support and efficient system maintenance of the computing team at the AIfA.

References

Aarseth S. J., 2003, Gravitational N-Body Simulations, Cambridge University Press, Cambridge, UK, pp. 430. ISBN 0521432723
Aarseth S. J., 2012, MNRAS, 422, 841
Abbott B. P., et al., 2019, Physical Review X, 9, 031040
Abdul-Masih M., et al., 2019, arXiv e-prints, p. arXiv:1912.04092
Banerjee S., 2017, MNRAS, 467, 524
Banerjee S., 2018, MNRAS, 481, 5123
Banerjee S., Belczynski K., Fryer C. L., Berczik P., Hurley J. R., Spurzem R., Wang L., 2019, arXiv e-prints, p. arXiv:1902.07718
Belczynski K., Kalogera V., Rasio F. A., Taam R. E., Zezas A., Bulik T., Maccarone T. J., Ivanova N., 2008, The Astrophysical Journal Supplement Series, 174, 223
Belczynski K., Bulik T., Fryer C. L., Ruiter A., Valsecchi F., Vink J. S., Hurley J. R., 2010, The Astrophysical Journal, 714, 1217
Belczynski K., et al., 2016, A&A, 594, A97
Belczynski K., et al., 2017, arXiv e-prints, p. arXiv:1706.07053
Belczynski K., et al., 2019, arXiv e-prints, p. arXiv:1911.12357
Blandford R. D., Znajek R. L., 1977, MNRAS, 179, 433
Crowther P. A., Schnurr O., Hirschi R., Yusof N., Parker R. J., Goodwin S. P., Kassim H. A., 2010, MNRAS, 408, 731
De Donder E., Vanbeveren D., 2004, New Astron. Rev., 48, 861
De Mink S. E., Mandel I., 2016, MNRAS, 460, 3545
De Mink S. E., Cantiello M., Langer N., Pols O. R., Brott I., Yoon S.-C., 2009, A&A, 497, 243
De Mink S. E., Sana H., Langer N., Izzard R. G., Schneider F. R. N., 2014, ApJ, 782, 7
Di Carlo U. N., Giacobbo N., Mapelli M., Pasquato M., Spera M., Wang L., Haardt F., 2019, arXiv e-prints, p. arXiv:1901.00863
El-Badry K., Quataert E., 2019, arXiv e-prints, p. arXiv:1912.04185
Fryer C. L., Belczynski K., Wiktorowicz G., Dominik M., Kalogera V., Holz D. E., 2012, ApJ, 749, 91
Fuller J., Piro A. L., Jermyn A. S., 2019, MNRAS, 485, 3661
Gaburov E., Lombardi J. C., Portegies Zwart S., 2008, MNRAS, 383, L5
Giacobbo N., Mapelli M., Spera M., 2018, MNRAS, 474, 2959
Giesers B., et al., 2018, MNRAS, 475, L15
Giesers B., et al., 2019, A&A, 632, A3
Hobbs G., Lorimer D. R., Lyne A. G., Kramer M., 2005, MNRAS, 360, 974
Hurley J. R., Pols O. R., Tout C. A., 2000, Monthly Notices of the Royal Astronomical Society, 315, 543
Hurley J. R., Tout C. A., Pols O. R., 2002, Monthly Notices of the Royal Astronomical Society, 329, 897
Hypki A., Giersz M., 2013, MNRAS, 429, 1221
Joshi K. J., Rasio F. A., Portegies Zwart S., 2000, ApJ, 540, 969
Kroupa P., 2001, MNRAS, 322, 231
Küpper A. H. W., Maschberger T., Kroupa P., Baumgardt H., 2011, MNRAS, 417, 2300
Langer N., Norman C. A., de Koter A., Vink J. S., Cantiello M., Yoon S. C., 2007, A&A, 475, L19

Lattimer J. M., Yahil A., 1989, ApJ, 340, 426
Liu J., et al., 2019, arXiv e-prints, p. arXiv:1911.11989
Marchant P., Langer N., Podsiadlowski P., Tauris T. M., Moriya T. J., 2016, A&A, 588, A50
Paxton B., Bildsten L., Dotter A., Herwig F., Lesaffre P., Timmes F., 2011, ApJS, 192, 3
Paxton B., et al., 2015, ApJS, 220, 15
Ramachandran V., et al., 2019, A&A, 625, A104
Rodriguez C. L., Chatterjee S., Rasio F. A., 2016, Physical Review D, 93
Sana H., Evans C. J., 2011, in Neiner C., Wade G., Meynet G., Peters G., eds, IAU Symposium Vol. 272, Active OB Stars: Structure, Evolution, Mass Loss, and Critical Limits. pp 474–485 (arXiv:1009.4197), doi:10.1017/S1743921311011124
Sana H., et al., 2013, A&A, 550, A107
Spera M., Mapelli M., Bressan A., 2015, Mon. Not. R. Astron. Soc., 451, 4086
Spera M., Mapelli M., Giacobbo N., Trani A. A., Bressan A., Costa G., 2019, MNRAS, 485, 889
Spitzer L., 1987, Dynamical evolution of globular clusters, Princeton University Press, Princeton, NJ, 191 p.
Thompson T. A., et al., 2019, Science, 366, 637
Thorne K. S., Zytkow A. N., 1975, ApJ, 199, L19
Thorne K. S., Price R. H., MacDonald D. A., 1986, Black holes: The membrane paradigm
Toonen S., Hamers A., Portegies Zwart S., 2016, Computational Astrophysics and Cosmology, 3, 6
Wang L., Spurzem R., Aarseth S., Nitadori K., Berczik P., Kouwenhoven M. B. N., Naab T., 2015, Monthly Notices of the Royal Astronomical Society, 450, 4070
Weidner C., Kroupa P., 2004, MNRAS, 348, 187
Woosley S. E., 2017, ApJ, 836, 244
de Mink S. E., Langer N., Izzard R. G., Sana H., de Koter A., 2013, ApJ, 764, 166

APPENDIX A: EXAMPLES OF TYPICAL BINARY-EVOLUTIONARY HISTORIES LEADING TO MASSIVE BLACK HOLES AT SOLAR AND SUB-SOLAR METALLICITIES

In the following, individual examples from the present `BSE` binary-evolutionary models, leading to exotic BH masses, are provided. In all these cases, the F12-rapid remnant-formation model (including B16-PPSN/PSN) and $f_{\rm mrg} = 0.2$ (Sec. 2) are applied. The stellar wind mass loss is always according to the B10 prescription except in Example 3a where 20% of this wind is applied. The `SSE` time step parameters of $(\texttt{pts1}, \texttt{pts2}, \texttt{pts3}) = (0.001, 0.01, 0.02)$ are applied in all cases.

Example 1a ($Z = 0.02$, $f_{\rm TZ} = 0.9$, $\alpha = 3.0$)**:**

```
NS/BH formation (mechanism/fallback control) MASS KS FBFAC FBTOT MCO VKICK KMECH:
5.7393168333929676   14  0.62576939152049149        5.3770187037699637
7.3172588535468650        197.14296511276697    1
```

TIME	M1	M2	K1	K2	SEP	ECC	R1/ROL1	R2/ROL2	TYPE
0.0000	44.451	66.882	1	1	78.729	0.19	0.368	0.401	INITIAL
3.2806	41.324	54.557	1	1	78.914	0.00	0.648	1.001	BEG RCHE
3.8856	44.232	48.716	1	2	75.743	0.00	0.777	1.465	KW CHNGE
3.8903	48.963	43.958	1	4	72.412	0.00	0.733	81.084	KW CHNGE
3.8918	59.374	33.534	1	4	81.898	0.00	0.577	88.638	BEG BSS
3.8942	74.135	18.751	1	4	158.043	0.00	0.266	0.450	END RCHE
3.8978	74.143	18.674	1	7	158.022	0.00	0.266	0.032	KW CHNGE
4.4266	70.247	9.919	1	8	182.610	0.00	0.241	0.022	KW CHNGE
4.4535	70.045	5.739	1	14	96.990	0.90	0.424	0.000	KW CHNGE
4.4535	70.045	5.739	1	14	96.935	0.90	0.424	0.000	CONTACT
4.4535	68.780	9.919	14	15	0.000	0.00	0.000	-1.000	COELESCE
13000.0000	68.780	0.000	14	15	0.000	-1.00	0.000	-1.000	MAX TIME

Note: with $f_{\rm TZ} = 0.9$, the final BH mass $= 5.739 M_\odot + (70.045 M_\odot \times 0.9) = 68.780 M_\odot$.

Example 1b ($Z = 0.02$, $f_{\rm TZ} = 0.9$, $\alpha = 3.0$)**:**

```
NS/BH formation (mechanism/fallback control) MASS KS FBFAC FBTOT MCO VKICK KMECH:
6.0403669764522627   14  0.63587200393794840        5.7115188627247360
7.6300772770290646        196.20808369097909    1
```

TIME	M1	M2	K1	K2	SEP	ECC	R1/ROL1	R2/ROL2	TYPE
0.0000	39.218	163.208	1	1	95.036	0.20	0.366	0.506	INITIAL
2.2629	39.065	105.439	1	1	87.277	0.00	0.493	1.001	BEG RCHE
3.2821	70.793	51.518	1	2	62.362	0.00	0.744	2.116	KW CHNGE
3.2865	76.465	45.798	1	4	64.706	0.00	0.710	105.578	KW CHNGE
3.2902	101.985	20.230	1	4	159.736	0.00	0.268	0.914	END RCHE
3.2956	101.949	20.171	1	7	159.790	0.00	0.268	0.036	KW CHNGE
3.3427	101.387	18.630	1	7	162.759	0.00	0.263	0.035	BEG BSS
3.8053	95.552	10.324	1	8	184.707	0.00	0.235	0.024	KW CHNGE
3.8312	95.213	6.040	1	14	105.972	0.80	0.385	0.000	KW CHNGE
3.8312	95.213	6.040	1	14	105.911	0.80	0.385	0.000	CONTACT
3.8312	91.732	10.324	14	15	0.000	0.00	0.000	-1.000	COELESCE
13000.0000	91.732	0.000	14	15	0.000	-1.00	0.000	-1.000	MAX TIME

Note: with $f_{\rm TZ} = 0.9$, the final BH mass $= 6.040 M_\odot + (95.213 M_\odot \times 0.9) = 91.732 M_\odot$.

Example 2a ($Z = 0.0001$, $f_{\rm TZ} = 0.0$, $\alpha = 3.0$)**:**

TIME	M1	M2	K1	K2	SEP	ECC	R1/ROL1	R2/ROL2	TYPE
0.0000	182.918	21.690	1	1	1227.847	0.20	0.017	0.015	INITIAL
3.1533	180.026	21.688	2	1	1245.455	0.20	0.023	0.017	KW CHNGE
3.1540	179.941	21.688	2	1	1245.944	0.20	1.001	0.017	BEG RCHE
3.1540	84.025	21.688	7	1	17.855	0.00	1.001	0.017	COMENV
3.1540	84.025	21.688	7	1	17.855	0.00	0.383	0.973	END RCHE
3.2029	83.625	21.692	7	1	17.405	0.00	0.392	1.000	BEG RCHE
3.3449	82.129	21.709	7	1	17.477	0.00	0.387	1.000	END RCHE
3.3576	81.971	21.710	15	1	0.000	0.00	0.000	-1.000	NO REMNT
9.0197	0.000	21.699	15	2	0.000	-1.00	-1.000	0.000	KW CHNGE
9.0359	0.000	21.699	15	4	0.000	-1.00	-1.000	0.000	KW CHNGE
9.8854	0.000	21.172	15	5	0.000	-1.00	-1.000	0.000	KW CHNGE
9.8928	0.000	19.036	15	14	0.000	-1.00	-1.000	0.000	KW CHNGE
13000.0000	0.000	19.036	15	14	0.000	-1.00	-1.000	0.000	MAX TIME

Example 2b ($Z = 0.0001$, $f_{\rm TZ} = 0.0$, $\alpha = 1.0$)**:**

TIME	M1	M2	K1	K2	SEP	ECC	R1/ROL1	R2/ROL2	TYPE
0.0000	182.918	21.690	1	1	1227.847	0.20	0.017	0.015	INITIAL
3.1533	180.026	21.688	2	1	1245.455	0.20	0.023	0.017	KW CHNGE
3.1540	179.941	21.688	2	1	1245.944	0.20	1.001	0.017	BEG RCHE
3.1540	174.972	21.688	2	15	6.009	0.00	1.001	0.017	COMENV
3.1541	174.952	0.000	4	15	0.000	-1.00	0.000	-1.000	KW CHNGE
3.4342	132.942	0.000	5	15	0.000	-1.00	0.000	-1.000	KW CHNGE
3.4430	180.026	0.000	15	15	MAX TIME	0.00	0.000	-2.000	NO REMNT

Example 2c ($Z = 0.001$, $f_{\rm TZ} = 0.0$, $\alpha = 3.0$)**:**

TIME	M1	M2	K1	K2	SEP	ECC	R1/ROL1	R2/ROL2	TYPE
0.0000	182.918	21.690	1	1	1227.847	0.20	0.019	0.018	INITIAL
3.1757	113.436	21.688	2	1	1857.539	0.20	0.038	0.012	KW CHNGE
3.1769	113.270	21.689	2	1	1859.623	0.20	1.001	0.012	BEG RCHE
3.1769	53.126	21.689	7	1	34.248	0.00	1.001	0.012	COMENV
3.1769	53.126	21.689	7	1	34.248	0.00	0.165	0.524	END RCHE
3.4405	40.500	21.733	14	1	41.525	0.09	0.000	0.411	KW CHNGE
3.4405	40.500	21.733	14	1	41.501	0.09	0.000	0.411	BEG SYMB
8.9310	40.518	21.668	14	1	40.936	0.00	0.000	1.001	BEG RCHE
9.0679	40.519	21.665	14	1	40.934	0.00	0.000	0.981	END RCHE
9.0679	40.519	21.665	14	1	40.934	0.00	0.000	0.981	BEG SYMB
9.0941	40.519	21.665	14	2	40.995	0.00	0.000	0.838	KW CHNGE
9.0963	40.519	21.664	14	2	41.004	0.00	0.000	1.001	BEG RCHE
9.1091	40.522	21.471	14	4	41.674	0.00	0.000	2.815	KW CHNGE
9.6953	40.809	7.693	14	4	203.643	0.00	0.000	0.655	END RCHE
9.6953	40.809	7.693	14	4	203.643	0.00	0.000	0.655	BEG SYMB
9.7154	40.815	7.682	14	7	203.593	0.00	0.000	0.018	KW CHNGE
9.7154	40.815	7.682	14	7	203.593	0.00	0.000	0.018	BEG SYMB
9.9688	40.816	7.600	14	8	203.931	0.00	0.000	0.016	KW CHNGE
10.0068	40.816	1.818	14	13	33.618	7.07	0.000	-2.000	DISRUPT
13000.0000	40.816	1.818	14	13	0.000	-1.00	0.000	0.000	MAX TIME

Example 3a ($Z = 0.0001$, $f_{\rm TZ} = 0.0$, $\alpha = 3.0$)**:**

TIME	M1	M2	K1	K2	SEP	ECC	R1/ROL1	R2/ROL2	TYPE
0.0000	198.903	104.554	1	1	63.895	0.50	0.431	0.454	INITIAL
2.4086	197.215	104.291	1	1	46.743	0.00	0.759	1.001	BEG RCHE
3.1312	196.235	103.562	1	1	47.017	0.00	0.729	1.459	BEG BSS
3.1349	196.238	103.546	2	1	47.319	0.00	0.618	1.454	KW CHNGE
3.1349	196.238	103.546	2	1	47.319	0.00	1.002	1.454	CONTACT
3.1349	299.784	103.546	2	15	7.965	0.00	0.990	0.990	COMENV
3.1353	299.779	0.000	4	15	0.000	-1.00	0.000	-1.000	KW CHNGE
3.4033	259.580	0.000	5	15	0.000	-1.00	0.000	-1.000	KW CHNGE
3.4081	232.983	0.000	14	15	0.000	-1.00	0.000	-1.000	KW CHNGE
13000.0000	232.983	0.000	14	15	0.000	-1.00	0.000	-1.000	MAX TIME

Example 3b ($Z = 0.02$, $f_{\rm TZ} = 0.0$, $\alpha = 3.0$, $0.2 \times$B10 wind)**:**

TIME	M1	M2	K1	K2	SEP	ECC	R1/ROL1	R2/ROL2	TYPE
0.0000	191.915	130.275	1	1	56.154	0.00	1.174	1.066	INITIAL
0.0000	191.915	130.275	1	1	56.154	0.00	1.174	1.066	BEG RCHE
0.0000	191.915	130.275	1	1	53.190	0.00	1.240	1.125	CONTACT
0.0000	296.135	130.275	1	15	0.000	0.00	0.000	-1.000	COELESCE
3.0270	205.443	0.000	2	15	0.000	-1.00	0.000	-1.000	KW CHNGE
3.0291	205.379	0.000	4	15	0.000	-1.00	0.000	-1.000	KW CHNGE
3.3598	195.457	0.000	5	15	0.000	-1.00	0.000	-1.000	KW CHNGE
3.3694	175.651	0.000	14	15	0.000	-1.00	0.000	-1.000	KW CHNGE
13000.0000	175.651	0.000	14	15	0.000	-1.00	0.000	-1.000	MAX TIME

Note: with $f_{\rm mrg} = 0.2$, the mass of the merger product $191.915 M_\odot + 130.275 M_\odot \times (1 - 0.2) = 296.135 M_\odot$.

Example 3c ($Z = 0.02$, $f_{TZ} = 0.0$, $\alpha = 3.0$)**:**

TIME	M1	M2	K1	K2	SEP	ECC	R1/ROL1	R2/ROL2	TYPE
0.0000	191.915	130.275	1	1	56.154	0.00	1.174	1.066	INITIAL
0.0000	191.915	130.275	1	1	56.154	0.00	1.174	1.066	BEG RCHE
0.0000	191.915	130.275	1	1	53.190	0.00	1.240	1.125	CONTACT
0.0000	296.135	130.275	1	15	0.000	0.00	0.000	-1.000	COELESCE
3.1652	62.867	0.000	2	15	0.000	-1.00	0.000	-1.000	KW CHNGE
3.1690	62.340	0.000	4	15	0.000	-1.00	0.000	-1.000	KW CHNGE
3.3890	29.340	0.000	7	15	0.000	-1.00	0.000	-1.000	KW CHNGE
3.5778	16.768	0.000	8	15	0.000	-1.00	0.000	-1.000	KW CHNGE
3.5813	14.968	0.000	14	15	0.000	-1.00	0.000	-1.000	KW CHNGE
13000.0000	14.968	0.000	14	15	0.000	-1.00	0.000	-1.000	MAX TIME